

Supporting Information

Matthews et al. 10.1073/pnas.1617526114

SI Text

1. Overview. Here, we provide additional materials in support of the text. In Fig. S1, we show how the sensitivity of the HI to changes in air temperature varies as a function of relative humidity and air temperature. Fig. S2 illustrates the 2D view of the projected heat stress changes that were averaged spatially in Fig. 3A. A list of the CMIP5 (13) model runs used in our analysis is provided below:

Group-model-rcp

BCC-BCC-CSM1.1-m-rcp45
BCC-BCC-CSM1.1-m-rcp60
BCC-BCC-CSM1.1-m-rcp85
BCC-BCC-CSM1.1-rcp45
BCC-BCC-CSM1.1-rcp60
BCC-BCC-CSM1.1-rcp85
BNU-BNU-ESM-rcp45
BNU-BNU-ESM-rcp85
CCCMA-CanESM2-rcp45
CCCMA-CanESM2-rcp85
CMCC-CMCC-CMS-rcp45
CMCC-CMCC-CM-rcp45
CMCC-CMCC-CM-rcp85
CNRM-CERFACS-CNRM-CM5-rcp45
CNRM-CERFACS-CNRM-CM5-rcp85
CSIRO-BOM-ACCESS1.0-rcp45
CSIRO-BOM-ACCESS1.0-rcp85
CSIRO-BOM-ACCESS1.3-rcp45
CSIRO-BOM-ACCESS1.3-rcp85
CSIRO-QCCCE-CSIRO-Mk3.6.0-rcp45
CSIRO-QCCCE-CSIRO-Mk3.6.0-rcp60
FIO-FIO-ESM-rcp45
FIO-FIO-ESM-rcp60
FIO-FIO-ESM-rcp85
ICHEC-EC-EARTH-rcp45
ICHEC-EC-EARTH-rcp85
INM-INM-CM4-rcp45
INM-INM-CM4-rcp85
IPSL-IPSL-CM5A-LR-rcp45
IPSL-IPSL-CM5A-LR-rcp60
IPSL-IPSL-CM5A-LR-rcp85
IPSL-IPSL-CM5A-MR-rcp45
CMCC-CMCC-CMS-rcp85
CSIRO-QCCCE-CSIRO-Mk3.6.0-rcp85
IPSL-IPSL-CM5A-MR-rcp60
MIROC-MIROC-ESM-rcp85
MPI-M-MPI-ESM-MR-rcp85
NCAR-CCSM4-rcp45
IPSL-IPSL-CM5A-MR-rcp85
IPSL-IPSL-CM5B-LR-rcp45
IPSL-IPSL-CM5B-LR-rcp85

Cont.

Group-model-rcp

LASG-CESS-FGOALS-g2-rcp45
LASG-CESS-FGOALS-g2-rcp85
MIROC-MIROC-ESM-CHEM-rcp45
MIROC-MIROC-ESM-CHEM-rcp60
MIROC-MIROC-ESM-CHEM-rcp85
MIROC-MIROC-ESM-rcp45
MIROC-MIROC-ESM-rcp60
MIROC-MIROC5-rcp45
MIROC-MIROC5-rcp60
MIROC-MIROC5-rcp85
MOHC-HadGEM2-CC-rcp45
MOHC-HadGEM2-CC-rcp85
MOHC-HadGEM2-ES-rcp45
MOHC-HadGEM2-ES-rcp85
MPI-M-MPI-ESM-LR-rcp45
MPI-M-MPI-ESM-LR-rcp85
MPI-M-MPI-ESM-MR-rcp45
MRI-MRI-CGCM3-rcp45
MRI-MRI-CGCM3-rcp60
MRI-MRI-CGCM3-rcp85
NASA-GISS-GISS-E2-H-CC-rcp45
NASA-GISS-GISS-E2-H-rcp45
NASA-GISS-GISS-E2-H-rcp60
NASA-GISS-GISS-E2-H-rcp85
NASA-GISS-GISS-E2-R-CC-rcp45
NASA-GISS-GISS-E2-R-rcp45
NASA-GISS-GISS-E2-R-rcp60
NASA-GISS-GISS-E2-R-rcp85
NCAR-CCSM4-rcp60
NCAR-CCSM4-rcp85
NCC-NorESM1-ME-rcp45
NCC-NorESM1-ME-rcp60
NCC-NorESM1-ME-rcp85
NCC-NorESM1-M-rcp45
NCC-NorESM1-M-rcp60
NCC-NorESM1-M-rcp85
NIMR-KMA-HadGEM2-AO-rcp45
NSF-DOE-NCAR-CESM1-BGC-rcp45
NSF-DOE-NCAR-CESM1-BGC-rcp85
NSF-DOE-NCAR-CESM1-CAM5-rcp45
NSF-DOE-NCAR-CESM1-CAM5-rcp60
NSF-DOE-NCAR-CESM1-CAM5-rcp85
BNU-BNU-ESM-rcp45

Monthly mean air temperatures from all runs listed were used to compute the coefficients for pattern-scaling observed air temperatures. Runs highlighted in gray indicate those model runs with sufficient data availability to calculate the HI and the SWBGT at daily resolution.

In the following, *SI Text*, section 2 describes the methods used to bias correct the heat stress projections, whereas *SI Text*, section

3 explains the approach used to generate heat stress projections for specific city regions. Finally, an alternative to the transient CMIP5 runs for calculating changes to global heat stress is described in *SI Text*, section 4.

2. Bias Correction of CMIP5 Model Runs. The 1979–2005 WFDEI (38) observational record corresponds to the timing of the historical CMIP5 model integrations. This period was used to evaluate bias in the CMIP5 runs and define the necessary correction functions to infer projected heat stress threshold exceedances. Following ref. 15, CMIP5 output was adjusted, such that the number of exceedances of given thresholds for heat stress metrics matched observations exactly. A bias correction was applied to each model run and each cell of the $0.5^\circ \times 0.5^\circ$ WFDEI grid:

$$\hat{HI}_c = \hat{HI} + \delta, \quad [\text{S1}]$$

where subscript c denotes the corrected quantity and δ is given by

$$\delta = \begin{cases} 40.6 - q(\hat{HI}, q^{-1}(HI, 40.6)) : \max(HI) \geq 40.6 \\ q(HI, 0.99) - q(\hat{HI}, 0.99) : \max(HI) < 40.6 \end{cases} \quad [\text{S2}]$$

in which $q(\cdot)$ indicates the quantile function and $q^{-1}(\cdot)$ is its inverse. The primes indicate modeled quantities; no prime represents the observed field. This correction ensures that, where 40.6°C is exceeded in the observations, the same numbers of exceedances are found in the concurrent model runs by translating the distribution accordingly; for grid cells that did not exceed 40.6°C in the observations, the differences in the 99th percentiles were used to shift the distribution. In essence, the correction is a quasiquantile mapping approach, which focuses on the upper tail of the distribution. This technique was applied, because it provides efficiency given the large ensemble size, while simultaneously targeting the part of the distribution that is of particular interest. Use of constant corrections for the upper parts of the distribution is not uncommon in quantile mapping (44, 45). Note also that, to correct the SWBGT and DB distributions (Fig. 3A), the same correction procedure was applied but used thresholds of 35°C (SWBGT) and 37.6°C (DB).

Reduced data dimensionality permitted a more rigorous bias correction for the specific city regions mentioned in the text (*SI Text*, section 3). After observed and CMIP5 HI values were interpolated to the respective locations, the observations along with the 1979–2005 component of the CMIP5 simulations were used to define an empirical quantile-matching correction analogous to the method used in ref. 44 and at steps of 0.1%. This correction was subsequently used to correct the entirety of each CMIP5 series (1979–2099).

3. Heat Stress for City Regions. City HI values were obtained for the respective warming scenarios ($1.5^\circ\text{C} \dots 4.0^\circ\text{C}$) by extracting the relevant 30-y periods for each interpolated city/model series based on the proximity of the models' simulated global mean

temperature to the level of global warming targeted (more details of this procedure are in *Materials and Methods*). We defined cities as heat stressed under these warming amounts as those that were projected to experience $n\text{HI}40.6 \geq 1$ according to the ensemble median. For cities that entered this category for the first time in the respective warming scenario, we identified their closest historical analogs [both in terms of the number of days exceeding HI40.6 (frequency) and their 99.9th percentiles (intensity)] by finding the minimum absolute difference when the respective metric was compared with data from all other cities during the reference period. Cities already heat stressed during the 1979–2005 reference period are reported in Table S1, whereas those cities set to experience heat stress for the first time under the respective warming scenarios are listed in Tables S2–S4 along with their historical analogs. Note that, when moving from 1.5°C to 2°C , no cities become newly heat stressed, and therefore, there is no supporting table for the 2°C warming scenario.

4. Heat Stress from Pattern-Scaled Air Temperature. A second approach to estimating the sensitivity of global heat stress to air temperature changes was applied using an observation-based perturbation method (plotted as shifted HI in Fig. 3A). This technique reveals the extent to which heat stress changes are sensitive to uniform increases in air temperature across the distribution along with no net change in relative humidity as suggested by CMIP5 models. Ref. 5 used a similar technique to explore the impact of global warming on heat stress (as measured by the SWBGT) from observations. This study extends the approach by acknowledging that the local temperature response resulting from global warming is far from homogeneous. This effect was accommodated by pattern-scaling the local temperature response. Specifically, monthly coefficients relating the local to global temperature change were obtained by separately regressing the running 30-y mean monthly temperature at each grid cell onto the running 30-y global mean air temperature. The slope coefficient (β) of this regression yields the sensitivity of local monthly air temperature to global mean air temperature change. These regressions were computed on each model's native grid and interpolated to the $0.5^\circ \times 0.5^\circ$ grid of the observations. The impacts of given global mean air temperature changes (ΔT_g) on global heat stress were then assessed by translating each warming scenario to a local response. That is, HI values were calculated with relative humidity unchanged, and the daily temperatures at grid cell i in month m was calculated according to

$$\hat{T}_{i,m} = T_{i,m} + \overline{\beta_{i,m}} \Delta T_g,$$

where the prime indicates the perturbed state of the observed daily series and the overbar denotes the mean across the CMIP5 ensemble. Note that, because of greater data availability of monthly fields, a larger CMIP5 ensemble was used to calculate $\overline{\beta_{i,m}}$ than was used to evaluate HI directly from daily data. The list of model runs used is given in the table in *SI Text*, section 1, whereas $\overline{\beta_{i,m}}$ is shown in Fig. S3.

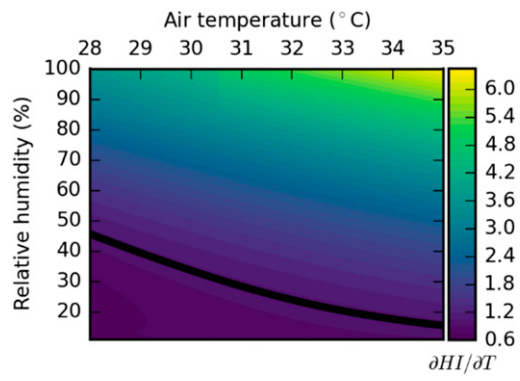


Fig. S1. Results from numerically differentiating HI with respect to air temperature for different values of relative humidity and air temperature. The black line is the unity contour; along this line, a 1 °C change in air temperature is accompanied by a 1 °C change in the HI.

Table S2. Projected changes in HI for city regions becoming heat stressed (in the text) under a climate 1.5 °C above PI (not experiencing heat stress during the 1979–2005 reference period)

City, country	Ref nHI40.6 (d a ⁻¹)	Proj nHI40.6 (d a ⁻¹)	NN nHI40.6 (city, country)	Ref HI99.9 (°C)	Proj 99.9 (°C)	NN HI99.9 (city, country)
Mumbai, India	0.9	10.4	Khartoum, Sudan	41.2	43.3	Hanoi, Vietnam
Shanghai, China	0.2	2.3	Karachi, Pakistan	39.7	42.5	Karachi, Pakistan
Lagos, Nigeria	0.1	7.8	Delhi, India	40.0	42.2	Karachi, Pakistan
Guangzhou, China	0.8	9.1	Khartoum, Sudan	41.3	43.8	Dhaka, Bangladesh
Ho Chi Minh, Vietnam	0.0	3.0	Surat, India	39.3	41.7	Surat, India
Chittagong, Bangladesh	0.5	5.6	Lahore, Pakistan	40.9	43.1	Ahmedabad, India
Yangon, Myanmar	0.1	2.4	Karachi, Pakistan	39.2	42.0	Surat, India
Abidjan, Ivory Coast	0.4	18.8	Kolkata, India	40.7	42.8	Ahmedabad, India

nHI40.6 and HI99.9 inherit their meanings from Table S1. NN highlights the city in the WFDEI dataset (1979–2005) with the respective HI statistic most similar to the projected conditions (i.e., its spatial analog). For example, in this +1.5 °C climate, Lagos is projected to have, on average, nHI40.6 = 7.8 according to the ensemble median, which is most similar to the frequency of threshold exceedances experienced by Delhi during the reference period (WFDEI data; 1979–2005). HI99.9, 99.9th percentiles in HI; NN, nearest neighbor; Proj, ensemble median climate model projections; Ref, statistics from the reference WFDEI (1979–2005).

Table S3. The same as in Table S2 but for cities becoming heat stressed at 2.7 °C above PI air temperatures

City, country	Ref nHI40.6 (d a ⁻¹)	Proj nHI40.6 (d a ⁻¹)	NN nHI40.6 (city, country)	Ref HI99.9 (°C)	Proj 99.9 (°C)	NN HI99.9 (city, country)
Tokyo, Japan	0	2.0	Karachi, Pakistan	35.8	42.4	Karachi, Pakistan
Beijing, China	0	1.9	Karachi, Pakistan	37.1	43.2	Hanoi, Vietnam
Manila, the Philippines	0	5.9	Lahore, Pakistan	37.2	42.7	Ahmedabad, India
Jakarta, Indonesia	0	6.8	Lahore, Pakistan	37.0	42.3	Karachi, Pakistan
Hyderabad, India	0	3.6	Ahmedabad, India	38.1	43.1	Ahmedabad, India
Baghdad, Iraq	0	1.0	Mumbai, India	37.5	41.4	Guangzhou, China
Pune, India	0	4.8	Ahmedabad, India	37.8	42.4	Karachi, Pakistan
Luanda, Angola	0	1.0	Mumbai, India	35.7	41.6	Guangzhou, China
Aleppo, Syria	0	1.2	Mumbai, India	36.8	41.3	Guangzhou, China

HI99.9, 99.9th percentiles in HI; NN, nearest neighbor; Proj, ensemble median climate model projections; Ref, statistics from the reference WFDEI (1979–2005).

Table S4. The same as in Table S2 but for cities becoming heat stressed at 4.0 °C above PI air temperatures

City, country	Ref HI > 40.6 (d a ⁻¹)	Proj HI > 40.6 (d a ⁻¹)	NN HI40.6 (city, country)	Ref HI99.9 (°C)	Proj 99.9 (°C)	NN HI99.9 (city, country)
New York, the United States	0	5.0	Ahmedabad, India	33.2	44.2	Dhaka, Bangladesh
Rio de Janeiro, Brazil	0	4.7	Ahmedabad, India	34.7	43.5	Hanoi, Vietnam
Kinshasa, DRC	0	36.4	Kolkata, India	34.9	45.6	Khartoum, Sudan
Bangalore, India	0	7.1	Hanoi, Vietnam	33.5	43.3	Hanoi, Vietnam
Riyadh, Saudi Arabia	0	8.1	Bangkok, Thailand	35.6	43.9	Dhaka, Bangladesh
Alexandria, Egypt	0	8.7	Khartoum, Sudan	33.8	44.4	Lahore, Pakistan

DRC, Democratic Republic of Congo; HI99.9, 99.9th percentiles in HI; NN, nearest neighbor; Proj, ensemble median climate model projections; Ref, statistics from the reference WFDEI (1979–2005).